PHYSICAL REVIEW LETTERS **131,** 011801 (2023)

Simultaneous Measurement of Muon Neutrino ν_μ Charged-Current Single π^+ Production in CH, C, H_2O, Fe, and Pb Targets in MINERvA

A. Bercellie,[1] K. A. Kroma-Wiley,[2,1] S. Akhter,[3] Z. Ahmad Dar,[4,3] F. Akbar,[3] V. Ansari,[3] M. V. Ascencio,[5,*] M. Sajjad Athar,[3] L. Bellantoni,[6] M. Betancourt,[6] A. Bodek,[1] J. L. Bonilla,[7] A. Bravar,[8] H. Budd,[1] G. Caceres,[9,†] T. Cai,[1] G. A. Díaz,[1] H. da Motta,[9] S. A. Dytman,[10] J. Felix,[7] L. Fields,[11] A. Filkins,[4] R. Fine,[1,‡] A. M. Gago,[5] H. Gallagher,[12] P. K. Gaur,[3] A. Ghosh,[13,9] S. M. Gilligan,[14] R. Gran,[15] E. Granados,[7] D. A. Harris,[16,6] D. Jena,[6] S. Jena,[17] J. Kleykamp,[1,§] A. Klustová,[18] M. Kordosky,[4] D. Last,[2] T. Le,[12,19] A. Lozano,[9] X.-G. Lu,[20,21] I. Mahbub,[15] E. Maher,[22] S. Manly,[1] W. A. Mann,[12] C. Mauger,[2] K. S. McFarland,[1] B. Messerly,[10,∥] J. Miller,[13] O. Moreno,[4,7] J. G. Morfín,[6] D. Naples,[10] J. K. Nelson,[4] C. Nguyen,[23] A. Olivier,[1] V. Paolone,[10] G. N. Perdue,[6,1] K.-J. Plows,[21] M. A. Ramírez,[2,7] R. D. Ransome,[19] H. Ray,[23] D. Ruterbories,[1] H. Schellman,[14] C. J. Solano Salinas,[24] H. Su,[10] M. Sultana,[1] V. S. Syrotenko,[12] B. Utt,[15] E. Valencia,[4,7] N. H. Vaughan,[14] A. V. Waldron,[18] B. Yaeggy,[13,¶] and L. Zazueta[4]

(The MINERvA Collaboration)

[1]*Department of Physics and Astronomy, University of Rochester, Rochester, New York 14627, USA*
[2]*Department of Physics and Astronomy, University of Pennsylvania, Philadelphia, Pennsylvania 19104, USA*
[3]*AMU Campus, Aligarh, Uttar Pradesh 202001, India*
[4]*Department of Physics, William and Mary, Williamsburg, Virginia 23187, USA*
[5]*Sección Física, Departamento de Ciencias, Pontificia Universidad Católica del Perú, Apartado 1761, Lima, Perú*
[6]*Fermi National Accelerator Laboratory, Batavia, Illinois 60510, USA*
[7]*Campus León y Campus Guanajuato, Universidad de Guanajuato,*
Lascurain de Retana No. 5, Colonia Centro, Guanajuato 36000, Guanajuato México
[8]*University of Geneva, 1211 Geneva 4, Switzerland*
[9]*Centro Brasileiro de Pesquisas Físicas, Rua Dr. Xavier Sigaud 150, Urca, Rio de Janeiro, Rio de Janeiro, 22290-180, Brazil*
[10]*Department of Physics and Astronomy, University of Pittsburgh, Pittsburgh, Pennsylvania 15260, USA*
[11]*Department of Physics, University of Notre Dame, Notre Dame, Indiana 46556, USA*
[12]*Physics Department, Tufts University, Medford, Massachusetts 02155, USA*
[13]*Departamento de Física, Universidad Técnica Federico Santa María, Avenida España 1680 Casilla 110-V, Valparaíso, Chile*
[14]*Department of Physics, Oregon State University, Corvallis, Oregon 97331, USA*
[15]*Department of Physics, University of Minnesota—Duluth, Duluth, Minnesota 55812, USA*
[16]*York University, Department of Physics and Astronomy, Toronto, Ontario, M3J 1P3 Canada*
[17]*Department of Physical Sciences, IISER Mohali, Knowledge City, SAS Nagar, Mohali - 140306, Punjab, India*
[18]*The Blackett Laboratory, Imperial College London, London SW7 2BW, United Kingdom*
[19]*Rutgers, The State University of New Jersey, Piscataway, New Jersey 08854, USA*
[20]*Department of Physics, University of Warwick, Coventry, CV4 7AL, United Kingdom*
[21]*Oxford University, Department of Physics, Oxford, OX1 3PJ United Kingdom*
[22]*Massachusetts College of Liberal Arts, 375 Church Street, North Adams, Massachusetts 01247, USA*
[23]*University of Florida, Department of Physics, Gainesville, Florida 32611, USA*
[24]*Facultad de Ciencias, Universidad Nacional de Ingeniería, Apartado 31139, Lima, Perú*

(Received 16 September 2022; accepted 2 June 2023; published 6 July 2023)

Neutrino-induced charged-current single π^+ production in the $\Delta(1232)$ resonance region is of considerable interest to accelerator-based neutrino oscillation experiments. In this Letter, high statistic differential cross sections are reported for the semiexclusive reaction $\nu_\mu A \to \mu^- \pi^+ +$ nucleon(s) on scintillator, carbon, water, iron, and lead targets recorded by MINERvA using a wideband ν_μ beam with $\langle E_\nu \rangle \approx 6$ GeV. Suppression of the cross section at low Q^2 and enhancement of low T_π are observed in both light and heavy nuclear targets compared with phenomenological models used in current neutrino interaction generators. The cross sections per nucleon for iron and lead compared with CH

---

across the kinematic variables probed are 0.8 and 0.5 respectively, a scaling which is also not predicted by current generators.

DOI: 10.1103/PhysRevLett.131.011801

Charged pion production is an important process for accelerator-based oscillation experiments. For low energy experiments, T2K [1], T2HK [2], and SBN [3], this process is both a significant background to quasielastic scattering and is used as a signal reaction when the pion is identified. For higher energy experiments, NOvA [4] and DUNE [5], the process is a large fraction of the signal. Neutrino oscillation experiments rely on an accurate model of pion production to evaluate neutrino energy for events with charged pions. Although NOvA, T2K, and T2HK utilize relatively low-A nuclear media such as hydrocarbons or water, SBN and DUNE experiments rely on argon ($A = 40$) targets. In order for these experiments to make use of the wealth of neutrino interaction data obtained with light nuclei, a knowledge of neutrino cross section scaling as a function of target A is required. This Letter tests scaling behavior by simultaneously measuring the differential cross sections of $\nu_\mu + A \rightarrow \mu^- + \pi^+ +$ nucleons as the target nucleon number is changed from carbon ($A = 12$) to lead ($A = 208$). We also present ratios of cross sections on different targets to those on scintillator, where many systematic uncertainties cancel, allowing a precise measurement of the nuclear dependence.

Previous measurements of charged-current pion production [6–11] have found disagreements between data and models at both low Q^2 (the negative of the square of the four momentum transfer from the lepton) and in pion kinetic energy. Simulations of this process must model both the primary neutrino-nucleon interaction and a variety of nuclear effects, including interactions of produced hadrons within the nucleus. This convolution of primary production and nuclear modification makes it difficult to isolate the model features responsible for the disagreements. Measurements on multiple nuclei can help separate nuclear effects from other aspects of the interaction.

Signal reactions for this measurement are ν_μ charged-current interactions which produce a single negatively charged muon and a single positively charged pion. Any number of baryons may be in the final state; however, no other mesons may be produced. To match MINERvA's acceptance, the muon is restricted in momentum (p_μ) and angle with respect to the neutrino beam (θ_μ), such that $1.5 < p_\mu < 20\ \mathrm{GeV}/c$ and $\theta_\mu < 13°$. Pion kinetic energy (T_π) is restricted to $35 < T_\pi < 350$ MeV.

To enhance reactions involving a Δ baryon resonance, a selection is made on the invariant hadronic mass of the final state. We define $W_{\mathrm{exp}} = M^2 + 2ME_{\mathrm{had}} - Q^2$, where $E_{\mathrm{had}} = E_\nu - E_\mu$, M is the average of the proton and neutron masses. W_{exp} is the invariant mass of the hadronic final state under the assumption that the target nucleon is at rest. W_{exp} is required to be less than $1.4\ \mathrm{GeV}/c^2$.

This analysis provides measurements in eight kinematic variables: the magnitude of the muon momentum and its longitudinal and transverse components (p_μ, $p_{\mu,||}$, and $p_{\mu,T}$), the angle of the muon (θ_μ), the kinetic energy and angle of the charged pion with respect to the neutrino beam (T_π and θ_π), Q^2, and W_{exp} as defined by the kinematics of the final state particles.

These measurements use event samples collected at the MINERvA detector using the medium energy NuMI beam at Fermilab [12]. To create the neutrino beam, 120 GeV protons impact a graphite target and produce pions and kaons. Two magnetic horns focus these charged particles into a pipe where they decay into primarily muon neutrinos. A GEANT4 simulation of the NuMI beamline [13] predicts the neutrino flux using constraints from hadron production data. Previous MINERvA measurements of neutrino elastic scattering on atomic electrons, $\nu e^- \rightarrow \nu e^-$, constrain the normalization of the neutrino flux, reducing the uncertainty of the flux between 2 and 20 GeV from 7.8% to 3.9% [14,15]. Another MINERvA measurement of inverse muon decay, $\nu_\mu e^- \rightarrow \mu^- \nu_e$, constrains the flux at higher neutrino energies [16]. These data represent an exposure of 10.6×10^{20} protons on target, half of which were taken with the water target filled.

The MINERvA detector consists of a central polystyrene-based scintillator tracker with an upstream nuclear target region and downstream electromagnetic and hadronic calorimeters. The nuclear target region contains five planes of passive material comprised of carbon, water, iron, and lead targets. The scintillator tracking planes are 95% CH by weight. The passive targets are interspersed between regions of active tracking volumes. The finely segmented tracking volumes of the MINERvA detector consist of hexagonal planes of nestled triangular scintillator strips with a pitch of 1.7 cm, allowing for spatial reconstruction with a resolution of 3 mm [12]. The MINOS Near Detector, located 2 m downstream of the MINERvA detector measures charge and momentum of exiting muons [17].

The simulation of the MINERvA detector utilizes GEANT4 version 4.9.4p2 [18] with the QGSP_BERT physics list [19–21] to model the detector response. Calibrations using through-going muons provide the absolute energy scale [12]. Measurements on a scaled down version of the MINERvA detector in a charged particle test beam set the hadronic energy response [22]. Overlaying data onto simulated events captures the effects of overlapping activity due to additional beam interactions.

A modified version of the GENIE v2.12.6 event generator, denoted “MnvTune v4.3.1,” supplies the neutrino interaction simulation [23]. For inelastic events with the invariant hadronic mass $W < 1.7\ \mathrm{GeV}/c^2$, resonance pion production assumes the Rein-Seghal model [24] with an axial mass of $M_A^{\mathrm{RES}} = 1.12\ \mathrm{GeV}/c^2$ [25]. Deep inelastic scattering relies on the Bodek-Yang model [26] tuned to agree with external measurements of pion production and total cross sections. Coherent pion production is simulated with the Rein-Seghal [27,28] model with corrections for muon mass. The nuclear medium is modeled as a relativistic Fermi gas (with Fermi momentum $p_F \sim 250\ \mathrm{MeV}/c$) [29] with an added Bodek-Ritchie high momentum tail [30,31]. Simulation of hadron final state interactions within the nucleus is predicted by the INTRANUKE-hA package [23].

The GENIE simulation has been tuned to better reproduce MINERvA data and provide more accurate signal and background models. Modifications to the quasielastic process are described in Refs. [32,33]. Pion production through baryon resonances is modified to match the D_2 bubble chamber data as in Ref. [34]. Coherent pion production is reweighted in both the energy of the pion E_π and θ_π to agree with a recent measurement of coherent pion production [35]. The normalization of coherent pion production is increased by 43.7% to account for coherent interactions on hydrogen, known as diffractive pion production, based on the Kopeliovic model [36]. The changes above comprise “MnvTune v4.2.1.”.

However, signal events in the scintillator disagree with the prediction of this model. The model for all targets except hydrogen was corrected by matching the simulated cross section versus Q^2 to the data. This results in improved estimates of efficiencies and backgrounds. The correction decreases the single pion production for $Q^2 < 0.1\ \mathrm{GeV}^2/c^2$ with a slow logarithmic increase for higher Q^2. Details of this tune are given in the Supplemental Material [37]. This modification, combined with those of MnvTune v4.2.1, forms MnvTune v4.3.1.

Selected events are required to have at least two tracked particles that start in the correct target. One track must be identified as a negatively charged muon by the MINOS Near Detector. One remaining track must be identified as a noninteracting charged pion by matching a Michel electron to the endpoint of the track and having longitudinal energy deposition (dE/dx) consistent with a noninteracting pion. All remaining tracks must not have dE/dx consistent with a pion. The charged pion tracking efficiency decreases at lower momentum and at angles perpendicular to the detector axis. The efficiency to reconstruct the Michel electron from the μ^+ was predicted from the simulation and validated in the scintillator tracker using stopping muons produced in the rock upstream of the detector [38]. The $W_{\mathrm{exp}} < 1.4\ \mathrm{GeV}/c^2$ requirement strongly reduces the number of multipion events. Both W_{exp} and Q^2 are computed using the visible calorimetric energy in the detector to estimate E_{had} [38]. After all cuts there are 33 231 events in the tracker, 1403 (1033) events in the iron (lead), and 295 (291) events in the carbon (water).

The two primary backgrounds are pion production events with $W_{\mathrm{exp}} > 1.4\ \mathrm{GeV}/c^2$ and pion production events that appear to originate from the passive nuclear targets but are actually produced in the adjacent scintillator. First, simulated events with reconstructed $W_{\mathrm{exp}} > 1.4\ \mathrm{GeV}/c^2$ in the scintillator target are weighted to match data using two scale factors, one for events with true W_{exp} between 1.4 and $1.8\ \mathrm{GeV}/c^2$ and one for events with W_{exp} above $1.8\ \mathrm{GeV}/c^2$. True W_{exp} is computed in the same manner as reconstructed W_{exp} but uses true simulated values. To improve the background prediction from events in the scintillator adjacent to the passive target, pions with low T_π or $\theta_\pi > 90°$ also receive additional weights to improve agreement with the scintillator target data. Next, simulated events in each target are weighted to correct the prediction of adjacent scintillator backgrounds using events observed in data near the passive targets. Finally, a weight is applied for events with high reconstructed W_{exp}, in the same manner as above, for each target material. Figure 1 shows a sample of

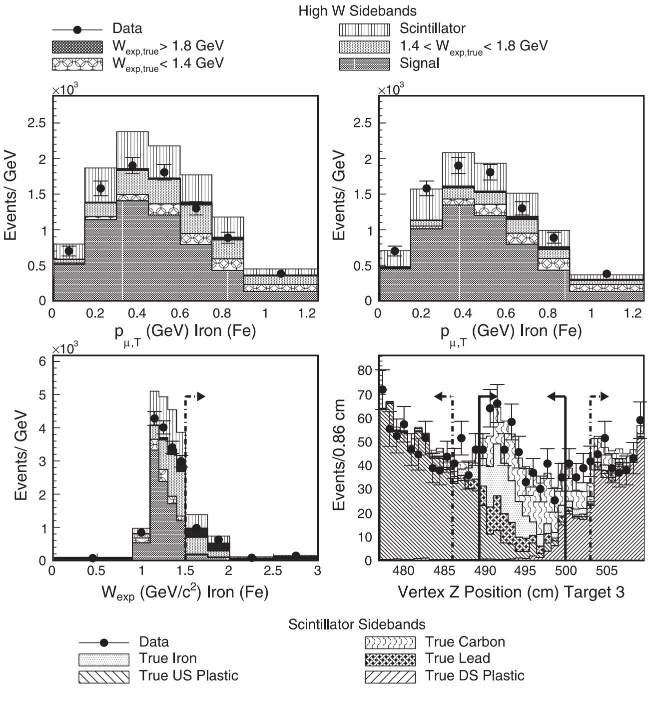

FIG. 1. $p_{\mu,T}$ distributions in iron for the signal regions before (top left) and after (top right) the simulation has been constrained with background estimates from data, the high W sideband in W_{exp} in iron (bottom left), and the scintillator sidebands in vertex z of target 3 (bottom right). The backgrounds in the bottom plots have not been constrained. The solid (dashed) arrows in the lower right plot delineate the signal (sideband) regions. Events labeled $W_{\mathrm{exp,true}} < 1.4$ GeV are those that pass the signal $W_{\mathrm{exp,true}}$ selection but fail other elements of the signal definition.

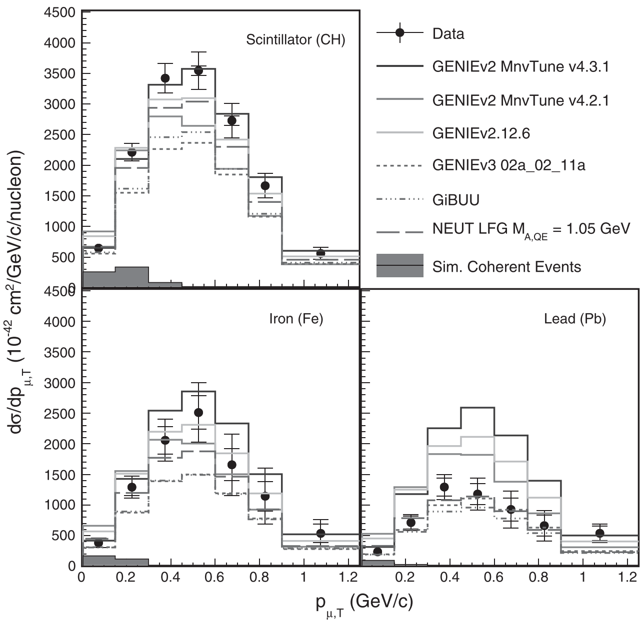

FIG. 2. Differential cross section $(d\sigma/dp_{\mu,T})$ measured on scintillator, iron, and lead (solid points) compared with GENIE, GIBUU, and NEUT generators, all of which are discrepant with one if not all nuclei.

data used in the background constraints, before and after constraints. The full set of weights is given in the Supplemental Material [37].

Kinematic smearing due to the detector in the background-subtracted distributions is removed with iterative D'Agostini unfolding [39,40] as implemented in the RooUnfold [41] framework. The number of iterations was chosen by studying the fidelity of unfolding randomly thrown pseudodata samples generated from alternate physics models. The event distributions are corrected for selection efficiency and acceptance, which is 4.5% (1%) on average in the tracker (passive targets). Efficiencies are available in the Supplemental Material [37]. The differential cross sections are obtained by normalizing the resulting event rates by the integrated neutrino flux and number of target nucleons.

One complication of forming ratios of cross sections between the passive targets and the tracker is that the fluxes have small differences due to the distributions of mass relative to the beam axis, as shown in the Supplemental Material [37]. This is corrected by measuring the cross section on scintillator in several regions of the detector, each integrated over a slightly different neutrino energy distribution. Linear combinations of these regional cross sections are used to form a cross section integrated over a flux that matches the relevant target. These cross sections are used to form the ratio of target-to-tracker cross section ratios [38,42].

Figures 2 and 3 show the differential cross sections $(d\sigma/dp_{\mu,T})$ and $(d\sigma/dT_{\pi})$, respectively, on materials with highest statistics (iron, lead, and scintillator). Lower statistic measurements on water and carbon are available in the Supplemental Material [37]. The statistical uncertainty dominates in all measurements, except in the scintillator. An example of the uncertainties on the cross sections is shown in Fig. 4; uncertainties in the cross section models which enter via efficiency and unfolding are the largest, but are lower than the statistical uncertainties in all targets but

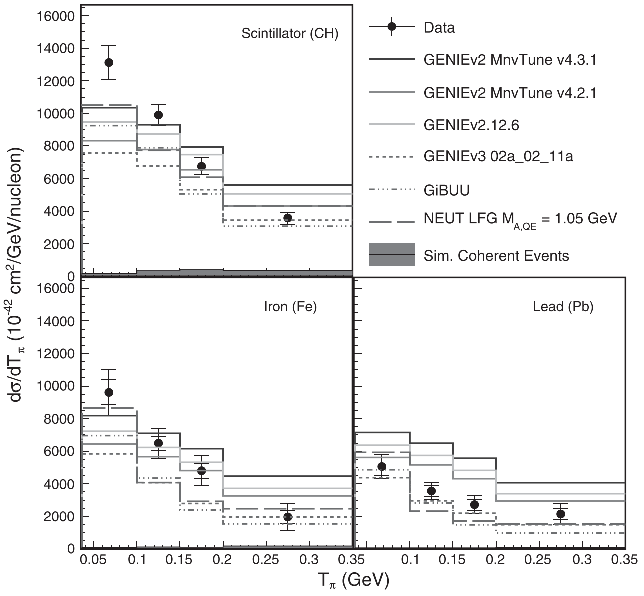

FIG. 3. Differential cross section $(d\sigma/dT_{\pi})$ in the scintillator, iron, and lead (solid points) compared with GENIE, GIBUU, and NEUT generators, all of which are discrepant.

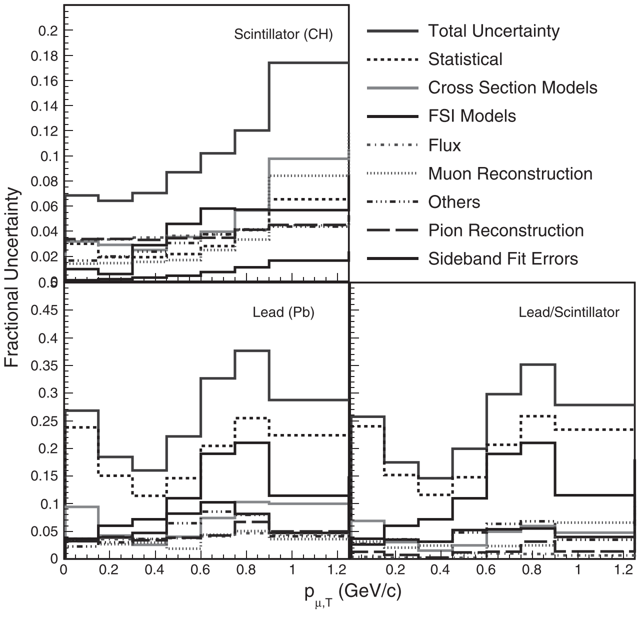

FIG. 4. Systematic uncertainties on the differential cross section $(d\sigma/dp_{\mu,T})$ in lead and scintillator and uncertainties of the ratio of $(d\sigma_{Pb}/dp_{\mu,T})/(d\sigma_{\mathrm{CH}}/dp_{\mu,T})$.

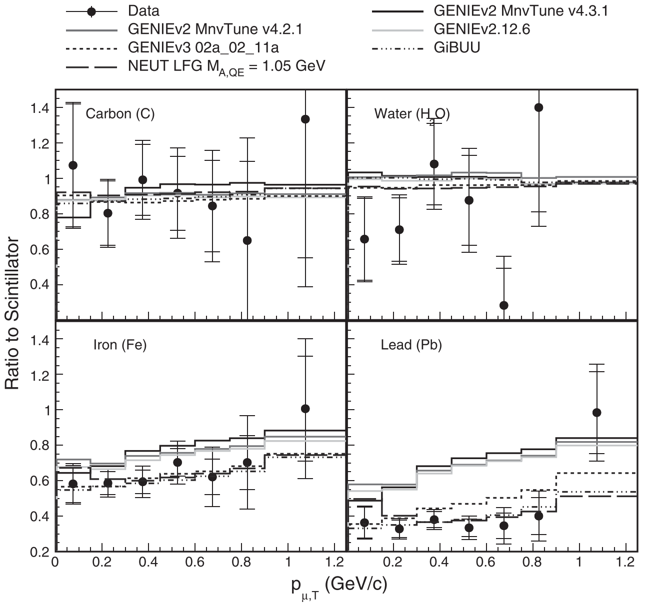

FIG. 5. Cross section ratios $(d\sigma_A/dp_{\mu,T})/(d\sigma_{\rm CH}/dp_{\mu,T})$ for carbon, water, iron, and lead (solid points), as compared to GENIE, NEUT, and GIBUU.

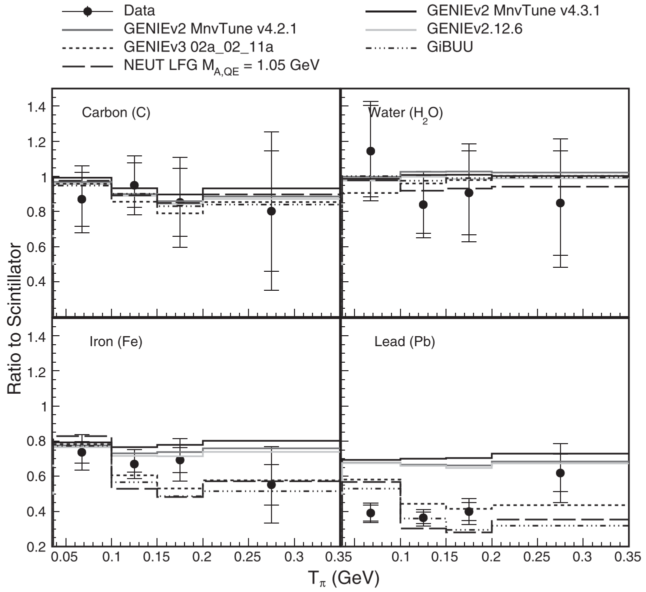

FIG. 6. Cross section ratios $(d\sigma_A/dT_{\pi^+})/(d\sigma_{\rm CH}/dT_{\pi^+})$ for carbon, water, iron, and lead (solid points) compared with predictions from GENIE, NEUT, and GIBUU. The predictions from GIBUU and NEUT agree better with the measurements than those from GENIE.

the scintillator. Statistical uncertainties in the sideband constraints are also significant for the passive targets. Systematic uncertainties are smaller in the cross section ratios, which benefit from partial cancellation of the flux, cross section model, and reconstruction uncertainties.

Ratios of cross sections to that in the scintillator are shown for $(d\sigma/dp_{\mu,T})$ and $(d\sigma/dT_\pi)$ in Figs. 5 and 6. The cross section ratios of carbon or water to the scintillator can be characterized by a scale factor of unity, while ratios between iron or lead to the scintillator are constant at 0.8 and 0.5 respectively, with no large modifications to distribution shapes for either $p_{\mu,T}$ or T_π. Cross sections and cross section ratios to the scintillator in other kinematic variables are tabulated and shown in the Supplemental Material [37]. Ratios in the other variables also exhibit this scaling behavior.

None of the six generator models investigated capture the evolution of absolute cross section. The generators NEUT [43] and GIBUU [44] do correctly predict the cross section ratios between Fe and Pb and the scintillator, as shown in Figs. 5 and 6, while the GENIE predictions do not agree. The GENIE models use pion- and nucleon-nucleus scattering data to implement single-step absorption and other scattering processes (INTRANUKE-hA) [23], whereas NEUT, NuWRO, and GIBUU employ different microscopic transport algorithms to simulate pion and nucleon intranuclear scattering.

As previously noted, the scintillator cross section showed a large discrepancy with the MINERvA-tuned GENIE model, which is corrected with a weight as a function of Q^2. In Fig. 2, the differential cross section as a function of the related observable $p_{\mu,T}$ $(Q^2 \approx p_{\mu,T}{}^2[1+\mathcal{O}(E_{\rm had}/E_\mu)])$ shows poor agreement both with untuned GENIE models (GENIEv2.12.6) and with tuned models without this weighting function (GENIEv2 MnvTune v4.2.1). The shape of the data is in better agreement with the weighted model (GENIEv2 MnvTune v4.3.1) in all targets, even though the weight is derived using only the scintillator measurement. The absolute normalization of the cross section is not well described by MnvTune v4.3.1 in iron or lead.

Similarly, the ratios of $d\sigma/dp_{\mu,T}$ between the targets and scintillator are consistent with being independent of $p_{\mu,T}$. A feature of both the GENIE v3 and GiBUU models is that they predict the large suppression lead relative to other targets. However, as seen in Fig. 6, these models also predict a larger ratio at low T_π in the heavy targets, a feature which is not seen in the data.

In summary, these data on single pion production on a wide variety of nuclei provide a new way to test nuclear models through their nuclear dependence. We observe a large modification to the predicted Q^2 distribution of single π^+ events that can be consistently seen in all nuclei. These results give guidance as to how the wealth of data on scintillator targets can be applied to models for oxygen and argon for future neutrino experiments.

This document was prepared by members of the MINERvA Collaboration using the resources of the Fermi National Accelerator Laboratory (Fermilab), a U.S. Department of Energy, Office of Science, HEP User Facility. Fermilab is managed by Fermi Research

Alliance, LLC (FRA), acting under Contract No. DE-AC02-07CH11359. These resources included support for the MINERvA construction project, and support for construction also was granted by the United States National Science Foundation under Award No. PHY-0619727 and by the University of Rochester. Support for participating scientists was provided by NSF and DOE (USA); by CAPES and CNPq (Brazil); by CoNaCyT (Mexico); by ANID PIA/APOYO AFB180002, CONICYT PIA ACT1413, and Fondecyt 3170845 and 11130133 (Chile); by CONCYTEC (Consejo Nacional de Ciencia, Tecnología e Innovación Tecnológica), DGI-PUCP (Dirección de Gestión de la Investigación—Pontificia Universidad Católica del Peru), and VRI-UNI (Vice-Rectorate for Research of National University of Engineering) (Peru); NCN Opus Grant No. 2016/21/B/ST2/01092 (Poland); by Science and Technology Facilities Council (UK); by EU Horizon 2020 Marie Skłodowska-Curie Action; by a Cottrell Postdoctoral Fellowship from the Research Corporation for Scientific Advancement; and by an Imperial College London President's PhD Scholarship. We thank the MINOS Collaboration for use of its near detector data. Finally, we thank the staff of Fermilab for support of the beam line, the detector, and computing infrastructure.

---

[*] Present address: Iowa State University, Ames, Iowa 50011, USA.

[†] Present address: Department of Physics and Astronomy, University of California at Davis, Davis, California 95616, USA.

[‡] Present address: Los Alamos National Laboratory, Los Alamos, New Mexico 87545, USA.

[§] Present address: Department of Physics and Astronomy, University of Mississippi, Oxford, Mississippi 38677, USA.

[∥] Present address: University of Minnesota, Minneapolis, Minnesota 55455, USA.

[¶] Present address: Department of Physics, University of Cincinnati, Cincinnati, Ohio 45221, USA.

[1] K. Abe *et al.* (T2K Collaboration), Nucl. Instrum. Methods Phys. Res., Sect. A **659**, 106 (2011).

[2] K. Abe *et al.* (Hyper-Kamiokande Collaboration), arXiv:1805.04163.

[3] M. Antonello *et al.* (MicroBooNE, LAr1-ND, ICARUS-WA104 Collaborations), arXiv:1503.01520.

[4] D. S. Ayres *et al.* (NOvA Collaboration), arXiv:hep-ex/0503053.

[5] R. Acciarri *et al.* (DUNE Collaboration), arXiv:1512.06148.

[6] A. A. Aguilar-Arevalo *et al.* (MiniBooNE Collaboration), Phys. Rev. D **83**, 052007 (2011).

[7] P. Adamson *et al.* (MINOS Collaboration), Phys. Rev. D **91**, 012005 (2015).

[8] B. Eberly *et al.* (MINERvA Collaboration), Phys. Rev. D **92**, 092008 (2015).

[9] T. Le *et al.* (MINERvA Collaboration), Phys. Lett. B **749**, 130 (2015).

[10] C. L. McGivern *et al.* (MINERvA Collaboration), Phys. Rev. D **94**, 052005 (2016).

[11] O. Altinok *et al.* (MINERvA Collaboration), Phys. Rev. D **96**, 072003 (2017).

[12] L. Aliaga *et al.* (MINERvA Collaboration), Nucl. Instrum. Methods Phys. Res., Sect. A **743**, 130 (2014).

[13] L. Aliaga *et al.* (MINERvA Collaboration), Phys. Rev. D **94**, 092005 (2016); **95**, 039903(A) (2017).

[14] E. Valencia *et al.* (MINERvA Collaboration), Phys. Rev. D **100**, 092001 (2019).

[15] L. Zazueta *et al.* (MINERvA Collaboration), Phys. Rev. D **107**, 012001 (2023).

[16] D. Ruterbories *et al.* (MINERvA Collaboration), Phys. Rev. D **104**, 092010 (2021).

[17] D. G. Michael *et al.* (MINOS Collaboration), Nucl. Instrum. Methods Phys. Res., Sect. A **596**, 190 (2008).

[18] S. Agostinelli *et al.* (GEANT4 Collaboration), Nucl. Instrum. Methods Phys. Res., Sect. A **506**, 250 (2003).

[19] M. P. Guthrie, R. G. Alsmiller, and H. W. Bertini, Nucl. Instrum. Methods **66**, 29 (1968).

[20] H. W. Bertini and M. P. Guthrie, Nucl. Phys. **A169**, 670 (1971).

[21] A. B. Kaidalov, Phys. Lett. **116B**, 459 (1982).

[22] L. Aliaga *et al.* (MINERvA Collaboration), Nucl. Instrum. Methods Phys. Res., Sect. A **789**, 28 (2015).

[23] C. Andreopoulos *et al.* (GENIE Collaboration), Nucl. Instrum. Methods Phys. Res., Sect. A **614**, 87 (2010).

[24] D. Rein and L. M. Sehgal, Ann. Phys. (N.Y.) **133**, 79 (1981).

[25] K. S. Kuzmin, V. V. Lyubushkin, and V. A. Naumov, Acta Phys. Pol. B **37**, 2337 (2006) [arXiv:hep-ph/0606184].

[26] A. Bodek, I. Park, and U.-K. Yang, Nucl. Phys. B, Proc. Suppl. **139**, 113 (2005).

[27] D. Rein and L. M. Sehgal, Nucl. Phys. **B223**, 29 (1983).

[28] D. Rein and L. Sehgal, Phys. Lett. B **657**, 207 (2007).

[29] E. J. Moniz, I. Sick, R. R. Whitney, J. R. Ficenec, R. D. Kephart, and W. P. Trower, Phys. Rev. Lett. **26**, 445 (1971).

[30] A. Bodek and J. L. Ritchie, Phys. Rev. D **23**, 1070 (1981).

[31] A. Bodek and J. L. Ritchie, Phys. Rev. D **24**, 1400 (1981).

[32] M. Carneiro *et al.* (MINERvA Collaboration), Phys. Rev. Lett. **124**, 121801 (2020).

[33] P. A. Rodrigues *et al.* (MINERvA Collaboration), Phys. Rev. Lett. **116**, 071802 (2016).

[34] P. Rodrigues, C. Wilkinson, and K. McFarland, Eur. Phys. J. C **76**, 474 (2016).

[35] M. A. Ramirez *et al.* (MINERvA Collaboration), arXiv:2210.01285.

[36] B. Z. Kopeliovich, I. Schmidt, and M. Siddikov, Phys. Rev. D **85**, 073003 (2012).

[37] See Supplemental Material at http://link.aps.org/supplemental/10.1103/PhysRevLett.131.011801 for additional cross sections, information about fluxes, and tables of the results in this manuscript.

[38] A. Bercellie (MINERvA Collaboration), Muon neutrino charged current single pion production on various targets

in the MINERvA detector, Ph.D. thesis, Rochester U., 2022, https://inspirehep.net/literature/2070948.
[39] G. D'Agostini, Nucl. Instrum. Methods Phys. Res., Sect. A **362**, 487 (1995).
[40] G. D'Agostini, in Alliance Workshop on Unfolding and Data Correction (2010), arXiv:1010.0632.
[41] T. Adye, in *PHYSTAT 2011* (CERN, Geneva, 2011), pp. 313–318, 10.5170/CERN-2011-006.313.
[42] J. Kleykamp, A-scaling of CCQE-like cross sections at MINERvA, Ph.D. thesis, Rochester U., Rochester U., 2021, https://inspirehep.net/literature/1936294.
[43] Y. Hayato, Acta Phys. Pol. B **40**, 2477 (2009), https://inspirehep.net/literature/844435.
[44] K. Gallmeister, U. Mosel, and J. Weil, Phys. Rev. C **94**, 035502 (2016).